

LETTER TO THE EDITOR

Discovery of the local counterpart of disc galaxies at $z > 4$: The oldest thin disc of Milky Way using Gaia-RVS

S. Nepal^{1,2}, C. Chiappini¹, A. B. Queiroz^{3,4}, G. Guiglion^{1,5,6}, J. Montalbán⁷, M. Steinmetz¹, A. Miglio⁷, A. Khalatyan¹

¹ Leibniz-Institut für Astrophysik Potsdam (AIP), An der Sternwarte 16, 14482 Potsdam, Germany
e-mail: snepal@aip.de

² Institut für Physik und Astronomie, Universität Potsdam, Karl-Liebknecht-Str. 24/25, 14476 Potsdam, Germany

³ Instituto de Astrofísica de Canarias, E-38205 La Laguna, Tenerife, Spain

⁴ Universidad de La Laguna, Departamento de Astrofísica, 38206 La Laguna, Tenerife, Spain

⁵ Zentrum für Astronomie der Universität Heidelberg, Landessternwarte, Königstuhl 12, 69117 Heidelberg, Germany

⁶ Max Planck Institute for Astronomy, Königstuhl 17, 69117, Heidelberg, Germany

⁷ Department of Physics & Astronomy, University of Bologna, Via Gobetti 93/2, 40129 Bologna, Italy

Received 31 January 2024 / accepted ...

ABSTRACT

Context. JWST has recently detected numerous disc galaxies at high-redshifts and there have been observations of cold disc galaxies at $z > 4$ with ALMA. In the Milky Way, recent studies highlight the presence of metal-poor stars in cold disc orbits, suggesting an ancient disc. This prompts a fundamental question: When did the Milky Way disc form, and did it originate as the thin disc or the larger velocity dispersion thick disc?

Aims. We do a chrono-chemo-dynamical study of a large sample of stars with precise stellar parameters, focusing on the oldest stars, to decipher the assembly history of the MW discs.

Methods. We investigated a sample of 565 606 stars with 6D phase space information and high-quality stellar parameters coming from the *hybrid*-CNN analysis of the *Gaia*-DR3 RVS stars. The sample contains 8 500 stars with $[\text{Fe}/\text{H}] < -1$. For a subset of $\sim 200\,000$ main sequence turnoff (MSTO) and subgiant branch (SGB) stars we computed distances and ages using the *StarHorse* code with a mean precision of 1% and 12%, respectively.

Results. First, we confirm the existence of metal-poor stars in thin disc orbits. The majority of these stars are predominantly old, with over 50% being older than 13 Gyr. Second, we report the discovery of the oldest thin disc of the Milky Way extending across a wide range of metallicities from metal-poor to super-solar stars. The metal-poor stars in disc orbits manifest as a readily visible tail of the metallicity distribution. We calculate the vertical velocity dispersion (σ_{V_z}) for the high- $[\alpha/\text{Fe}]$ thick disc as 35 km s^{-1} while the thin disc at same age range has a σ_{V_z} lower by 10 to 15 km s^{-1} . Our old thin disc σ_{V_z} appears similar to those estimated for the high- z disc galaxies. Third, as a verification of *StarHorse* ages, we extend the $[\text{Y}/\text{Mg}]$ chemical clock to the oldest ages and estimate a slope of $-0.038 \text{ dex} \cdot \text{Gyr}^{-1}$. Finally, we confirm our discovery of the old thin disc by showing that the *Splash* includes both old (> 9 Gyr) high- and low- $[\alpha/\text{Fe}]$ populations and extends to a wider $[\text{Fe}/\text{H}]$ range reaching super-solar $[\text{Fe}/\text{H}]$. We find about 6 to 10% of the old thin disc was heated to thick disc orbits. The youngest splashed stars appear at 9 to 10 Gyrs and possibly hint to the GSE merger at this period.

Conclusions. The Milky Way thin disc forms less than 1 billion years from Big Bang and continuously builds up in an inside out manner - this finding precedes the earlier estimates of start of the MW thin disc formation (around 8-9 Gyr) by about 4-5 billion years. We find that the metal-poor stars in disc orbits reported by previous studies belong to this old thin disc. Considering a massive merger event such as the GSE, a *Splash* is expected - we find a portion of the old thin disc is heated to thick disc velocities and the *Splash* extends to super-solar $[\text{Fe}/\text{H}]$ regimes.

Key words. Galaxy: abundances - Galaxy: evolution - Galaxy: kinematics and dynamics - stars: fundamental parameters - galaxies: evolution - galaxies: high-redshift

1. Introduction

The story of our Galaxy's childhood and adolescence, i.e. first few billion years after Big Bang, remains ambiguously portrayed in our Galactic saga. Deciphering the assembly history of the Milky Way is one of the main goals of Galactic Archaeology. To achieve this formidable goal, high-resolution chrono-chemo-kinematical maps of the Galaxy are a necessary step (e.g. Miglio et al. 2017). The key challenge in pursuing this objective lies in constructing large

datasets of stars with precise stellar ages. A common strategy to surmount this challenge involves focusing on very metal-poor stars, which offers a glimpse into the early stages of our Galaxy's evolution.

Very metal-poor stars are expected to trace the in-situ halo, debris from past merger events (such as GSE) and the so-called metal-weak thick disk (i.e. metal-poor tail of the chemical thick disk, MWTD - Norris et al. 1985; Morrison 1990; Chiba & Beers 2000; Beers et al. 2002). However, recent studies focusing on very-metal poor stars have un-

veiled a non-negligible number of stars in dynamically cold disk orbits (Sestito et al. 2019, 2020; Fernández-Alvar et al. 2021; Mardini et al. 2022; Matsunaga et al. 2022; Carollo et al. 2023; Ardern-Arentsen et al. 2023).

The existence of an ancient, very metal-poor disk in the Milky Way (MW) has become a contentious subject. For example, Zhang et al. (2023) using a Gaia RVS sample covering a broad metallicity range ($-3.0 < [M/H] < +0.5$), but again focusing on the most metal-poor stars, did not find a significant population of very-metal poor stars on disk orbits (within 2.5 kpc from the Galactic plane) suggesting previous results to actually stem from the prograde halo component. In an alternative scenario, Li et al. (2023) explored the idea that the bar would be the mechanism responsible for placing metal-poor stars in prograde disk orbits. However, they concluded that this process could only partially account for observations. Another possibility, discussed in the literature, is that merger events, such as Gaia Enceladus, might compel old stars initially in dynamically hot orbits to transition onto more dynamically cold, rotationally supported orbits (see McCluskey et al. 2023 and references therein). On the other hand, Bellazzini et al. (2023), utilizing a large sample of metal-poor stars with precise phase-space parameters and photometric metallicities, found a bimodal distribution in the vertical angular-momentum distribution of prograde stars, hence suggesting the presence of two disk-like components.

Recent high-redshift observations ($z > 4$) offer a complementary view to this topic. Studies with the Atacama Large Millimeter/Submillimetre Array (ALMA) have found a large fraction of star-forming dynamically cold disks (e.g. Rizzo et al. 2020, 2021; Lelli et al. 2023; Roman-Oliveira et al. 2023). James Webb Space Telescope (JWST) observations have also brought to light the discs in galaxies in the early universe (e.g. Ferreira et al. 2022; Kartaltepe et al. 2023; Robertson et al. 2023). These observations imply an early on formation/settling of discs. Current cosmological simulations have been debating what would be the main mechanisms responsible for producing these early discs (see Hopkins et al. 2023 and references therein), but in general have difficulties in producing them. According to these works, MW-like early discs would be a rare event.

Do we discern any counterpart within the MW to the early cold disks that formed within 1 billion years from the Big Bang? Is it plausible that the recently identified very-metal-poor stars in disk orbits within the MW represent part of an ancient, undisturbed disk that predates the high-alpha thick disk? If this pristine disk indeed exists, what would be its metallicity and the alpha-to-iron abundance ratio? Current Galactic archaeology efforts have been unable to establish the existence of the MW's disk counterpart to what is currently observed at high redshift. This challenge persists because the focus until now has been mostly on kinematics and metallicity or, when utilizing age data, on samples that lack substantial age precision beyond 10 billion years (Xiang & Rix 2022; Conroy et al. 2022; Belokurov & Kravtsov 2022), and where the thick disk dominates. Here we show that reliable stellar ages to chronologically tie up the full story otherwise only visible in hazy glimpses are now achievable for a Gaia *crème-de-la-crème* sample, built from the third data release *Gaia*-DR3.

In this Letter, for the first time, we are able to demonstrate the existence of a very old thin disk, covering a broad metallicity range. We start by confirming the exis-

tence of a metal-poor thin disc. We then are able to study the early disc using a chrono-chemo-dynamical analysis of a large sample of main-sequence turnoff (MSTO) and subgiant (SGB) stars selected from the RVS-CNN catalog of Guiglion et al. (2024), to which we add very precise distances and precise isochrone ages using *StarHorse*, In Sect. 2, we describe our sample focusing on the methods used to obtain the stellar ages and kinematics. In Sect. 3 we present our results and in Sect. 4 we present the main conclusions.

2. Data

Our sample is built from about one million spectra from the Radial Velocity Spectrometer (RVS)¹ which was analyzed by Guiglion et al. (2024, G23) using a hybrid Convolutional Neural-Network (hybrid-CNN) method, to derive precise atmospheric parameters (T_{eff} , $\log(g)$, and overall $[M/H]$) and chemical abundances ($[Fe/H]$ and $[\alpha/M]$)².

To select stars reliably parameterized by the hybrid-CNN method (see G23 for details) we adopt 'flag_boundary'='00000000'. We clean any spurious measurements by applying following uncertainty limits: 'sigma_teff' < 100 K, 'sigma_logg' < 0.1, 'sigma_feh' < 0.2 for $[Fe/H] \leq -0.5$ and 'sigma_feh' < 0.1 for $[Fe/H] > -0.5$ and 'sigma_alpham' < 0.05. We remove any stars with poor astrometric solutions by limiting 'RUWE' < 1.4, and we also remove known variable stars by using *Gaia* flag 'phot_variable_flag' ≠ 'VARIABLE' (see Gaia Collaboration et al. 2023). We compute the extinctions, distances and stellar ages with the *StarHorse* Bayesian isochrone-fitting method (Queiroz et al. 2018, 2023) and integrate the orbits of the stars using Galpy (Bovy 2015). For details on these computations see Appendix A.

We select stars with relative distance uncertainty less than 10% and extinction uncertainty less than 0.2 Mag. From this "full sample" we extract a sub-sample, which we name "age sample", consisting of MSTO and SGB stars (see Queiroz et al. 2023 for selection condition) with relative age uncertainty less than 25%. We keep only the MSTO and SGB stars as the stellar ages from isochrone fitting methods are most reliable for these evolutionary stages (e.g. Soderblom 2010). This sample however can be contaminated by low-luminosity giants and main-sequence stars which can have much larger age uncertainties. Adopting a more restrictive selection of MSTO+SGB (which leads to half the current age sample size) we still find the same results. In Appendix B we validate the *StarHorse* ages by extending the $[Y/Mg]$ chemical clock of Nissen et al. (2020) to the oldest ages, in addition to other tests with the stellar isochrones. Moreover, we compare the age-metallicity we obtain for a sub-sample of GSE-member candidates, with that of Limberg et al. (2022) obtained for GSE Globular Clusters and the GSE stars from Montalbán et al. (2021).

This gives us a sample of 565 606 stars with mean uncertainty of 2% for distance. Our age-sample consists 202 384

¹ The RVS spectra were originally analysed during *Gaia* DR3 (10.17876/gaia/dr.3) by the General Stellar Parametriser for spectroscopy (GSP-Spec, Recio-Blanco et al. 2023) module of the Astrophysical parameters inference system (Apsis, Creevey et al. 2023).

² We refer readers to G23 for details on the with significantly improved number of reliable targets with hybrid-CNN and improvements over GSP-Spec thanks to the novel method and inclusion of the additional information.

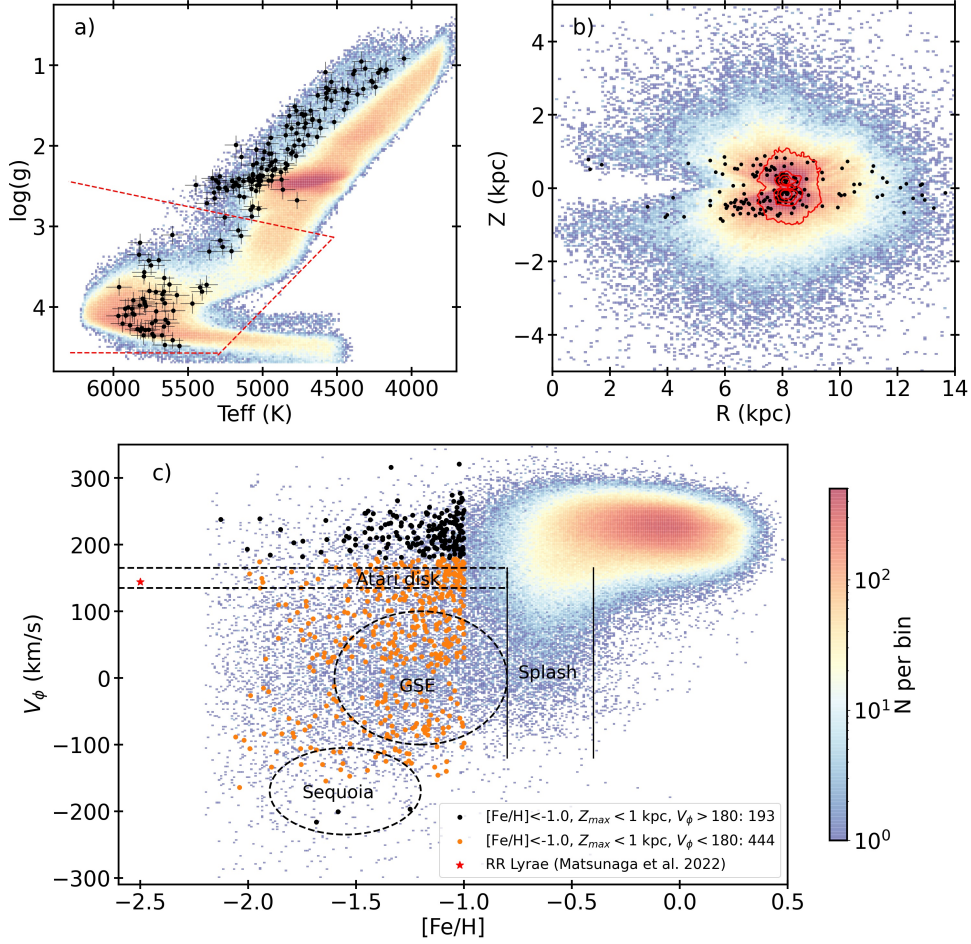


Fig. 1: Properties of the selected samples: a) the Kiel diagram ($\log(g)$ vs T_{eff}) for the full sample colour-coded by logarithm of stellar density. The dashed red lines represent the selection of MSTO+SGB stars (i.e. "age sample"). The black dots represent the metal-poor stars in thin disc like orbits (see legend in panel c) and the error bars show the uncertainties; b) Z vs R distribution of the full sample. The red contours show spatial extent of the age sample and the black dots show how the metal-poor stars in thin disc like orbits extend throughout the MW disc; c) Stars, from the full sample, in the V_{ϕ} vs $[\text{Fe}/\text{H}]$ plane. Several in-situ and ex-situ components of MW, namely GSE, Sequoia, Atari Disk and the Splash, are also illustrated in the plot. The black (orange) dots represent the metal-poor stars ($[\text{Fe}/\text{H}] < -1.0$) confined to $Z_{\text{max}} < 1$ kpc and with azimuthal velocity $> 180 \text{ km s}^{-1}$ ($< 180 \text{ km s}^{-1}$). The red star shows the RR Lyrae star found in SNd in disk orbit by Matsunaga et al. (2022). The metal-poor stars in thin disc like orbits (black dots) span the full disc of MW and will be discussed in detail in Sec. 3.1.

stars with mean uncertainty of 12% for age and 1% for distance. Such low uncertainties are obtained due to very low parallax errors in the extended Solar Neighbourhood (SNd) thanks to *Gaia* and the high-quality stellar parameters and abundances from the G23 catalog. We note that for stars older than 12 Gyr our uncertainties can be underestimated (See Appendix B.3).

In the upper panels of Fig. 1 we present our sample properties. The full sample consists of stars in a large range of evolutionary stages with wide range of metallicities ($-2.2 < [\text{Fe}/\text{H}] < 0.5$) including 8500 metal-poor ($[\text{Fe}/\text{H}] < -1.0$) stars. Our stars are widely distributed in Z vs R space reaching from inner to outer Galaxy. However, the number of stars in the age sample, shown by red contours, decreases as we move away from the SNd, as expected for a sample of MSTO+SGB stars (see Queiroz et al. 2023).

3. Results and discussion

3.1. The metal-poor thin disc unveiled

In Fig. 1 we present the metal-poor stars in thin disc orbits (black dots) from our full sample. We selected stars with $[\text{Fe}/\text{H}] < -1.0$, $Z_{\text{max}} < 1$ kpc and $V_{\phi} > 180 \text{ km s}^{-1}$ to obtain the metal-poor stars in thin disc orbits. In panel b we see that these metal-poor stars span a large range of Galactocentric radii. In panel c, we plot the azimuthal velocity (V_{ϕ}) as a function of $[\text{Fe}/\text{H}]$. In addition, to the metal-poor stars in thin disc orbits (black), we also show stars with slower V_{ϕ} (orange) along with illustrations to show the location of the well known in-situ and ex-situ components in the V_{ϕ} vs $[\text{Fe}/\text{H}]$ plane. The stars with lower V_{ϕ} , overlap in the space of the Atari disk/MWTD, the GSE, Sequoia and other possible merger components (e.g. see Dodd et al. 2023; Horta et al. 2023). However, the metal-poor stars in thin disc orbits, with $\overline{V_{\phi}} = 218 \pm 24 \text{ km s}^{-1}$, stand out

as a distinct population (see Sec. 3.3 for a discussion with chemical abundances).

Our full sample, thanks to the high quality and large statistics of the G23 catalogue, gives us a key advantage to make a stricter selection compared with previous attempts in the literature (i.e. $[\text{Fe}/\text{H}] < -1.0$, $Z_{\text{max}} < 1$ kpc and $V_\phi > 180 \text{ km s}^{-1}$). This clearly unveils the presence of a metal-poor thin disc. Considering all metal-poor stars with their orbits confined within 1 kpc from the Galactic mid-plane, the thin disc component comprises a significant 30%. In Appendix C.1 we show that even when we consider $Z_{\text{max}} < 3$ kpc to obtain a larger sample of 2950 MP ($-2.2 < [\text{Fe}/\text{H}] < -1.0$) stars, we observe a strong preference for prograde circular/disc-like orbits. We find more than 700 stars in low eccentricity and high V_ϕ orbits ($\text{ecc} < 0.3$ and $\overline{V}_\phi = 200 \pm 32 \text{ km s}^{-1}$) comprising 25% of the total. These results also confirm the presence of the metal-poor thin disc.

The metal-poor thin disc consists majority of stars older than 13 Gyr, while the stars with lower V_ϕ (i.e. orange in Fig. 1) show a significant fraction of stars younger than 13 Gyr (See Appendix C.2 for details). This result hints at an early assembly scenario (>13 Gyr) of the MW disc. In the next section, we explore the kinematics of our full age sample, analysing in bins of ages and $[\text{Fe}/\text{H}]$. Towards larger metallicity bins the contribution of thin and thick disks starts to increase, hence the only way to investigate if the metal-poor thin disc we found here extends towards larger metallicities is by having precise ages.

3.2. Discovery of Milky Way's oldest thin disc

In Fig. 2 we present the toomre diagram ($\sqrt{V_R^2 + V_\phi^2}$ vs. V_ϕ) for our age sample in bins of ages and metallicities. The panels are arranged from old to young ages from top to bottom and metal-poor to metal-rich from left to right. The dotted curves locate the kinematic boundaries for the canonical thin and thick discs. The top four rows (a-d) highlighted in light green represent very old ages (14–10 Gyr) and show the most novel results.

For the oldest age (14–13 Gyr), at the metal-poor regime, i.e. columns 1 and 2, as expected, we find stars in halo like orbits as well as accreted debris. Panels a-1 and a-2 show the metal-poor thin disc stars discussed in the Sec. 3.1. However, unexpectedly we find a significant number of these old stars in the canonical thin and thick disc orbits at all metallicities. The metal-poor thin disc, with ages > 13 Gyr, extends as a tail of this old disc which is already metal enriched with bulk of the stars between $-0.75 < [\text{Fe}/\text{H}] < 0.0$. With increase in $[\text{Fe}/\text{H}]$ the fraction of thin disc stars increases (as shown in panels a-3 to a-7).

As we move to age bins 13–11 Gyr, we see an increase in number of the most metal-poor stars ($[\text{Fe}/\text{H}] < -1.3$, panels b-1 and c-1) while the $-1.3 < [\text{Fe}/\text{H}] < -1.0$ range (panels b-2 and c-2) sees a decrease compared to the oldest bin. As most of these stars are in both prograde and retrograde halo orbits, this could be the contribution of both merger events as well as in-situ bulge/halo. In the $-1.0 < [\text{Fe}/\text{H}] < -0.75$ range (panels b-3 and c-3), we also see a decrease in number of stars with age, but with most of these stars in thick/thin disc orbits. Interestingly, $-0.75 < [\text{Fe}/\text{H}] < 0.0$ range (panels b-4:6 and c-4:6) sees a big increase in number, with most of the stars in thick/thin disc orbits and a significant fraction of stars in near-halo orbits (splash like orbits

- see next section). We also see a huge buildup of metal-rich ($0.0 < [\text{Fe}/\text{H}] < 0.5$, panels b-7 and c-7) stars, most of which are in thin disc orbits. At this age and $[\text{Fe}/\text{H}]$ regime, formation of the high- α /thick disc is expected (see Miglio et al. 2021; Queiroz et al. 2023 - see also next section).

In the 11–10 Gyr age bin, we find very few metal-poor ($[\text{Fe}/\text{H}] < -1.0$, panels d-1:2) stars most of which are in halo orbits. For $-1.0 < [\text{Fe}/\text{H}] < 0.0$ (panels d-3:6), we now find a decrease in number of stars compared to the upper row while the metal-rich ($0.0 < [\text{Fe}/\text{H}] < 0.5$, panel d-7) stars slightly increase in number. A smaller fraction of stars in near-halo/splash orbits are seen for $-1.0 < [\text{Fe}/\text{H}] < -0.25$ (panels d-3:5).

In the age bins < 10 Gyr (columns e to j) nearly all of the stars are in thin/thick disc orbits. Stars with $[\text{Fe}/\text{H}] < -1.0$ are nearly absent and the $-1.0 < [\text{Fe}/\text{H}] < -0.75$ bins (panels e:j-3) sees only 20 to 40 stars each. We find most of these stars have higher metallicity $[\text{Fe}/\text{H}] > -0.25$.

This discovery of the oldest thin disc brings forward the question of how reliable are the stellar ages and if these stars could be contaminants from the younger local thin disc population. In Appendix C.1 we check the distributions of guiding radius (R_g), eccentricity and Z_{max} and find that the significant fraction of our old disc stars have smaller R_g as expected for an older population as well as low eccentricity and Z_{max} (see Appendix C.1 for details). We also extensively validated the ages with the $[\text{Y}/\text{Mg}]$ chemical clock, with the age-metallicity relation for GSE-member candidates and with the stellar isochrones (see Appendix B). These validations support the large age-resolution achieved with our high-quality data.

In Appendix E we perform a validation with an external catalog of the high-resolution GALAH survey - the findings support our discovery.

In this section, we presented the discovery of the oldest disc of the Milky Way, by examining the velocity distribution across stellar ages. This disc consists of stars in a wide $[\text{Fe}/\text{H}]$ range, already reaching super-solar $[\text{Fe}/\text{H}]$. It is now also clear that the metal-poor thin disc discussed in Sec 3.1 is the extension of this oldest thin disc.

3.3. The Milky Way's high- z discs

In this section we investigate in more detail the chemodynamical properties of the old disks of the MW. Are there similarities to the properties of the recently detected high- z disks? In addition, in Sec. 3.3.1, we search for imprints of the oldest MW disk left in the *Splash* (Belokurov et al. 2020).

Figure 3 (panel a) shows the σ_V -age relation for the chemical (high- $[\alpha/\text{Fe}]$) thick disk (here defined as stars with $[\alpha/\text{Fe}]$ above 0.15 dex) and for the thin disk. At old ages, we find a high- $[\alpha/\text{Fe}]$ thick disc with a velocity dispersion of 35 km/s while the old thin disc has a value lower by around 10 to 15 km/s. This is similar to the results of Miglio et al. (2021), who also reported the chemical thick disk to have a systematic larger velocity dispersion with respect to that of the thin disk. The large velocity dispersion of the chemical thick disk measured by Miglio et al. (2021) is also shown in the figure (triangle). In this case an independent age method, based on asteroseismology, was used.

For comparison, we also show the recent estimates of the velocity dispersion in high-redshift disks as reported in Rizzo et al. (2021) (brown diamonds). There is a striking

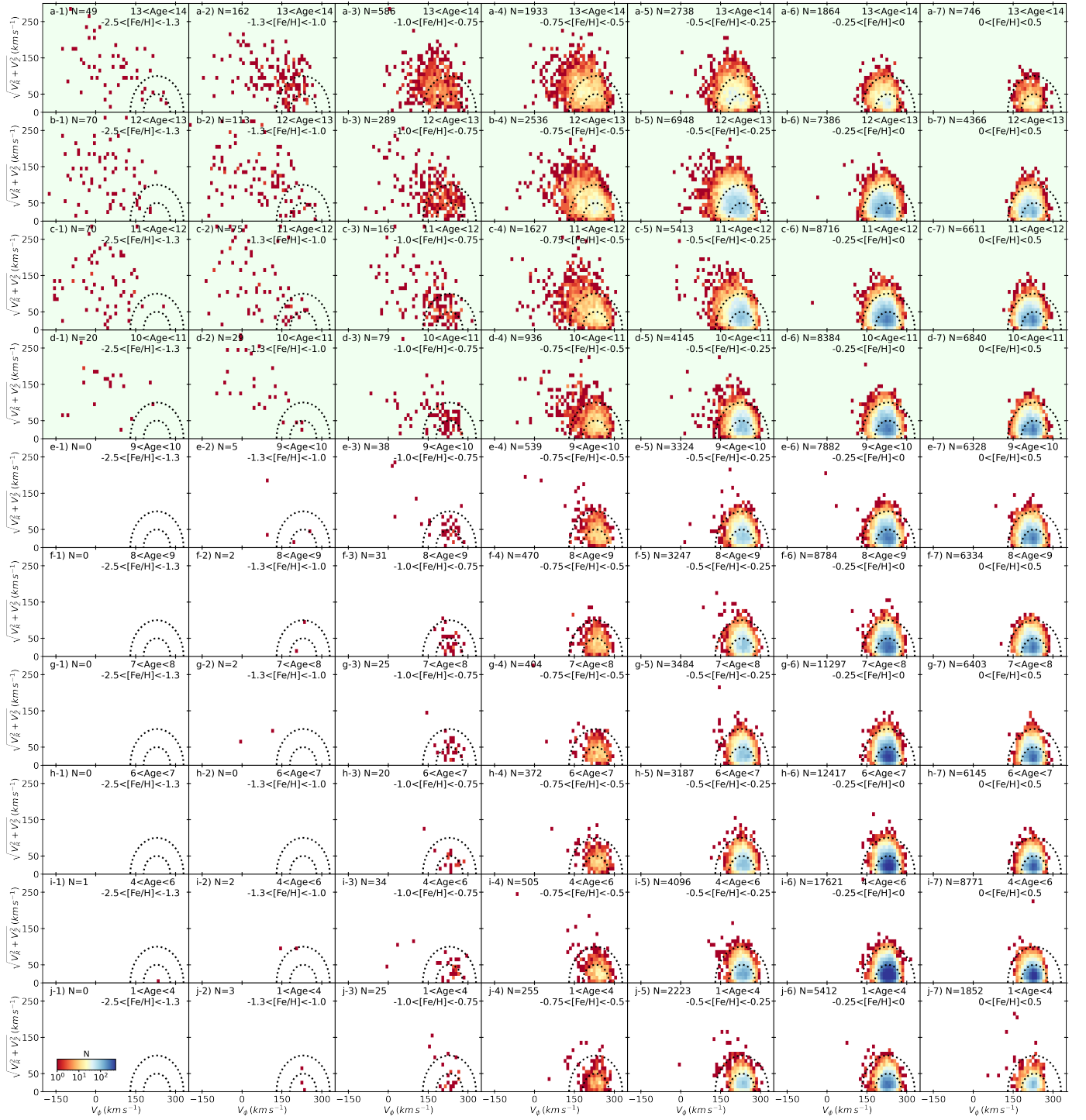


Fig. 2: Toomre diagrams ($\sqrt{V_R^2 + V_\phi^2}$ vs. V_ϕ) for the age sample stars in bins of age and $[\text{Fe}/\text{H}]$. The plots are color-coded by logarithm of stellar density. Older to younger ages from top to bottom and metal-poor to metal-rich $[\text{Fe}/\text{H}]$ from left to right. The age and $[\text{Fe}/\text{H}]$ range in each bin along with the respective number of stars is shown. The two dotted black curves represent the velocity boundaries for the thin ($|V_{\text{total}} - V_{\text{LSR}}| < 100 \text{ km s}^{-1}$) and thick ($100 \leq |V_{\text{total}} - V_{\text{LSR}}| < 200 \text{ km s}^{-1}$) discs. The top four rows highlighted in light green represent the very old ages (10 to 14 Gyr - showing the large age-resolution achievable with our data). As expected, at the oldest ages we find stars in halo like orbits as well as accreted debris. However, the unexpected result is the significant number of stars in canonical thin and thick disc orbits at all metallicities, extending to the old metal-poor disc discussed in Sec. 3.1.

similarity between these estimates and the values obtained for the old disks of the MW. The MW data gives not only support to an early settling of dynamically cold disk, but

also implies these disks to be stable over long timescales. As discussed in the Introduction, early disk settling is still a challenge to simulations, but see [Beraldo e Silva et al.](#)

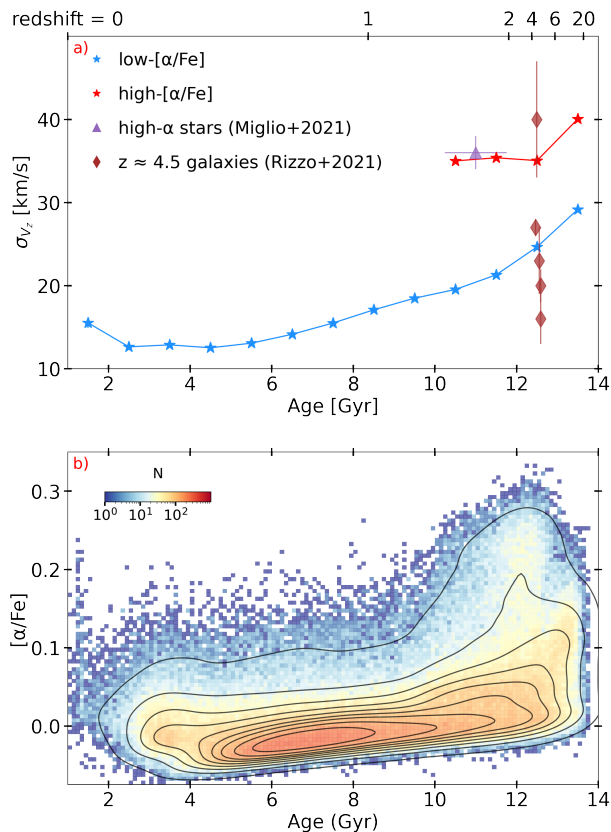


Fig. 3: Vertical velocity dispersion (σ_{V_z}) and $[\alpha/\text{Fe}]$ as a function of age. a): σ_{V_z} as a function of age for the high- $[\alpha/\text{Fe}]$ (red) and remaining disc (blue) stars. σ_{V_z} was measured in bins of 1 Gyr via the bootstrap resampling. The purple triangle represents the high- $[\alpha/\text{Fe}]$ stars from Miglio et al. (2021). The brown diamonds represent the velocity dispersion (σ_{ext}) for the high redshift galaxies ($z \approx 4.5$) from Rizzo et al. (2021). For the redshift to look-back age conversion $h = 0.7$, $\Omega_M = 0.3$, and $\Omega_\Lambda = 0.7$ is assumed (Planck Collaboration et al. 2016). b) Age- $[\alpha/\text{Fe}]$ relationship for the full age sample. A KDE is also overplotted to highlight the density features. The colours represent number of stars per bin in log scale.

(2021) and Kohandel et al. (2023). The latter authors do predict the existence of dynamically cold disks in the early phases of the universe evolution. Alternatively, Abadi et al. (2003) in their study of a hierarchical simulation find that an "old-thin disk" population can also be assembled via an edge-on accretion of the core of a satellite.

In Figure 3 (panel b) we show the $[\alpha/\text{Fe}]$ vs. age relation for our sample. At ages between 2 to 4 Gyr we find elevated $[\alpha/\text{Fe}]$ indicating enhanced star formation (SF) - this SF burst previously identified has recently been linked to the MW bar activity (see Nepal et al. 2024 and references therein). At ages past this SF burst, the figure shows a smooth increase of this abundance ratio with age, now extending to the first billion year of the universe evolution. The dataset hints for an older thin disk slightly less alpha enhanced than the chemical thick disk which forms later. Old low- $[\alpha/\text{Fe}]$ stars have been previously observed in small high-resolution spectroscopic samples (e.g. see Anders et al. 2018; Gent et al. 2022; Miglio et al. 2021; Vitali et al. 2024 and references therein), however absence of a

large statistics with precise ages has prohibited to identify and study the evolution of this old thin disc population. We refrain from a full age-chemical dissection for the high and low- $[\alpha/\text{Fe}]$ discs in the current work, first, because we lack multiple chemical species required for a reliable analysis for most of our stars and, second, because MSTO and SGB stars separately can have systematic difference in abundance (see Appendix B.3). In an upcoming work (Nepal et al. in prep) we perform a chemo-chrono-dynamical study of the MW discs with over 10 chemical species for a high-resolution spectroscopic sample.

In summary, thanks to our large sample of stars with precise ages, including more than 90 000 stars older than 9 Gyr, we are now able to unveil the oldest MW disk and to show it to be most probably distinct from the mostly coeval chemical thick disk. With previously available samples, only the chemical thick disk and the youngest part of the thin disk was seen.

3.3.1. Splashing the old thin and thick discs

A convincing test of our discovery of the oldest thin disc would be to check if the so-called *Splash* population contains also debris from this pristine stellar population. Belokurov et al. (2020), via a chemo-dynamical analysis of SNd stars, confirmed the presence of a population of metal-rich³ stars ($-0.7 < [\text{Fe}/\text{H}] < -0.2$) on highly eccentric orbits and named it as *Splash*. The authors argue that the splashed stars were born in MW's thick or protodisc prior to the last massive merger of GSE and have their orbits altered due to this merger event at around 9–10 Gyr ago.

In Fig. 4 we present stars in the V_ϕ vs. $[\text{Fe}/\text{H}]$ planes color-coded by stellar density. In panels a), b) and c) we plot the stars from our age sample. Panel a) shows old high- $[\alpha/\text{Fe}]$ (age > 9 Gyr and $[\alpha/\text{Fe}] > 0.15$)⁴ stars. We separate the groups at 9 Gyr as splashed stars disappear at younger ages. The magenta box shows the location for the canonical *Splash* population - we find high- $[\alpha/\text{Fe}]$ thick disc stars as expected (see Belokurov et al. 2020). In panel b) we show old and low- $[\alpha/\text{Fe}]$ (age > 9 Gyr and $[\alpha/\text{Fe}] < 0.15$) stars. Considering the wide $[\text{Fe}/\text{H}]$ range of the old thin disc, we extend in $[\text{Fe}/\text{H}]$ to define the low- $[\alpha/\text{Fe}]$ *Splash* region as $-100 < V_\phi < +100$ and $-1.0 < [\text{Fe}/\text{H}] < +0.5$. Similar to the high- $[\alpha/\text{Fe}]$ stars found in panel a), we find the old low- $[\alpha/\text{Fe}]$ stars in this region - most of the stars have $[\text{Fe}/\text{H}] < -0.2$ including a few stars with solar and super-solar $[\text{Fe}/\text{H}]$. We remind readers that the MSTO+SGB stars in our age sample are located close to SNd. We also note that at the metal-poor end around $[\text{Fe}/\text{H}] \approx -1.0$ dex, there could be contamination from merger remnants. Interestingly we also find a significant portion (about 10%) of the old low- $[\alpha/\text{Fe}]$ stars with thick disc kinematics. And in panel c) we show the low- $[\alpha/\text{Fe}]$ stars younger than 9 Gyr. Here we find the low- $[\alpha/\text{Fe}]$ *Splash* region nearly devoid of stars and only about 1.5% of stars with thick disc kinematics.

³ The authors consider stars with $-0.7 < [\text{Fe}/\text{H}] < -0.2$ as metal-rich as the halo populations usually found on high eccentricity orbits are metal-poor in comparison.

⁴ Considering possible systematic offset in abundances between MSTO and SGB stars (see Appendix B.3), we also test with $[\alpha/\text{Fe}] = 0.1$ to separate the high and low $[\alpha/\text{Fe}]$ populations and do not find any significant difference in the results.

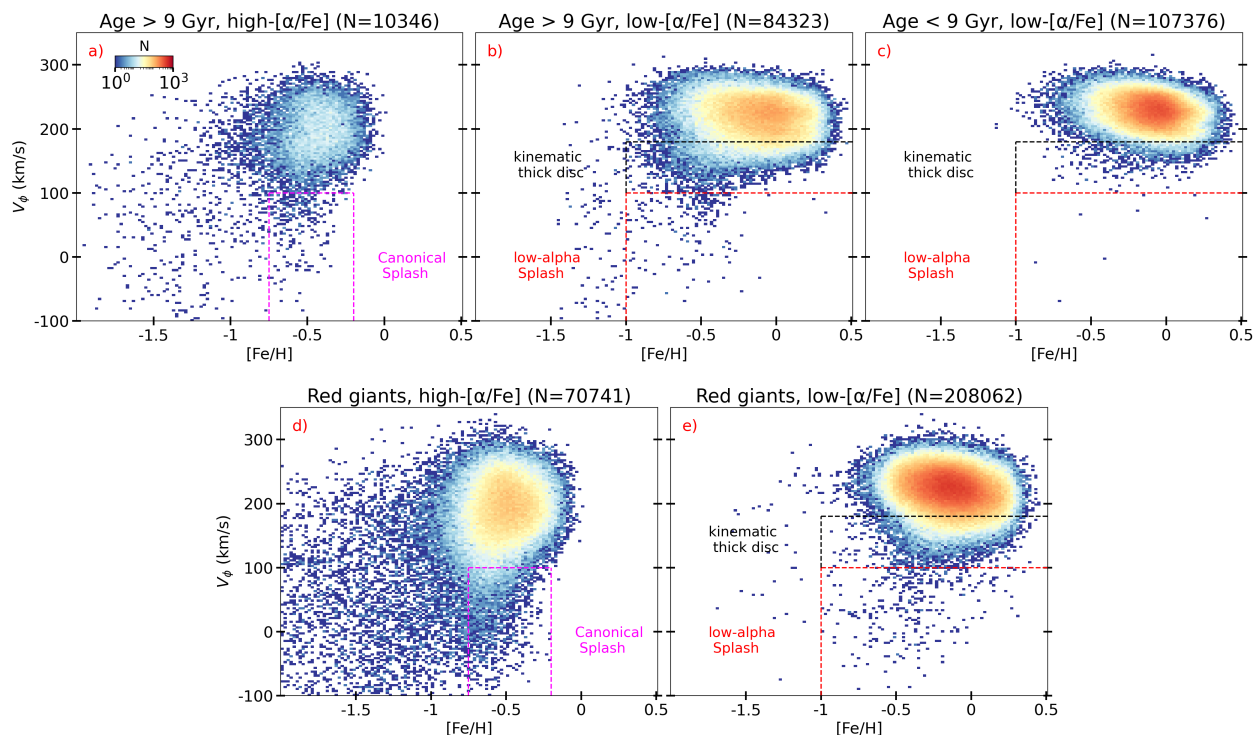


Fig. 4: V_ϕ vs. $[\text{Fe}/\text{H}]$ diagram for identification of Splash. The 2d density plots (panels a to e) are color-coded by number of stars per bin in log scale. The major debris contaminants, namely GSE and the Sagittarius, are excluded from these plots. Panels a, b and c show stars from the age sample while panels d and e shows red-giant stars with $\log(g) > 3$ from the full sample. In panels a and d we show the canonical Splash region (magenta box) defined by $-100 < V_\phi < +100$ and $-0.7 < [\text{Fe}/\text{H}] < -0.2$. In panels b, c and e show the region of kinematic thick disc (red box) defined by velocity $100 < V_\phi < +180$. We also define the low- $[\alpha/\text{Fe}]$ Splash region as $-100 < V_\phi < +100$ and $-1.0 < [\text{Fe}/\text{H}] < +0.5$.

In panels d) and e), we reconfirm the results from the age sample now with the larger sample of red giants. We limit stars to within 4 kpc from the sun to avoid contamination from the bulge/bar region. Based on the results from the age sample, we can divide the red -giants stars into high- and low- $[\alpha/\text{Fe}]$ groups and analyze the *Splash* population despite the unavailable age information in this case. Panel d) shows the splashed high- $[\alpha/\text{Fe}]$ stars similar to the old high- $[\alpha/\text{Fe}]$ population in panel a). And in panel e) the low- $[\alpha/\text{Fe}]$ stars also show signatures of the *Splash*. Thanks to the larger sample and wider spatial extent we now find more splashed stars from the "old" thin disc - there are more stars with solar and super-solar $[\text{Fe}/\text{H}]$. The fraction of low- $[\alpha/\text{Fe}]$ stars with thick disc kinematics is at about 6% - slightly lower than the value obtained with the age sample as now we cannot separate the old and young red-giant stars as in previously done in panel b) and c).

In this section we show that the *Splash* is comprised by both old (>9 Gyr) high- and low- $[\alpha/\text{Fe}]$ populations. We further report that a significant portion (about 6-10%) of the old thin disc was heated to thick disc kinematics supported by the absence of younger low- $[\alpha/\text{Fe}]$ at such azimuthal velocities.

4. Conclusion

In this Letter we explore the formation and evolution of the disc of the Milky Way, in light of recent observations of high- z disc galaxies, using 202 384 MSTO and SGB stars with 6D phase space information and high-quality stel-

lar parameters coming from the *Gaia*-DR3 RVS analysis of Guiglion et al. (2024). We supplemented the chemical abundances with stellar ages, distances, and kinematics - reaching the distance and age uncertainties of 1% and 12% thanks to *Gaia* DR3. Our main conclusions are the following:

- Thanks to the excellent age estimate by *StarHorse* based on the high-quality spectroscopic parameters from G23 and precise chemical abundances from GALAH survey we extend the $[\text{Y}/\text{Mg}]$ chemical clock to the oldest age regimes and estimate $d[\text{Y}/\text{Mg}]/d\text{Age}$ as $-0.038 \text{ dex} \cdot \text{Gyr}^{-1}$. This result is in agreement with previous analysis based on high-resolution spectroscopy and suggests our ages to be robust.
- We confirm the existence of the metal-poor stars in thin-disc orbits ($Z_{\text{max}} < 1$ kpc and $V_\phi > 180 \text{ km s}^{-1}$) reported by previous studies, now with the large statistics of the G23 spectroscopic sample. We show that over 50% of these metal-poor stars are older than 13 Gyr. These findings hint at an early formation of MW disc, and complement previous analysis focusing on larger distances from the galactic mid-plane (see Carter et al. 2021).
- We find the metal-poor old disc to give us only a partial view of an ancient disc. We discover that Milky Way's thin disc forms less than 1 billion years from Big Bang. This result precedes the earlier estimates (around 8–9 Gyr) of the start of MW thin disc formation by about 4–5 billion years. This old thin disc has an azimuthal velocity dispersion lower by 10 to 15 km s^{-1} compared

to 35 km s^{-1} of the high- $[\alpha/\text{Fe}]$ thick disc. We clearly see a thin disk extending to very old ages, on the top of a quenched thick disk (lasting around 1 Gyr only).

- We find that the *Splash* extends to the super-solar metallicities. We also find the presence (absence) of a significant fraction of low- $[\alpha/\text{Fe}]$ stars with thick disc kinematics older (younger) than 9 Gyr. Based on these results we confirm our discovery of the old thin disc and that the old thin disc was already in place before the last major merger of GSE which probably occurs at around 9 to 10 Gyrs ago (see discussion in [Gallart et al. 2019](#); [Naidu et al. 2021](#); [Montalbán et al. 2021](#)).

We have shown that Milky Way, similar to the high- z galaxies observed by JWST and by ALMA, has an old thin disc. The stars in this old disc ranges from metal-poor ($[\text{Fe}/\text{H}] < -1.0$) to those already enriched to super-metal-rich metallicities ($[\text{Fe}/\text{H}] \approx 0.25$) – this hints at an intense star formation and very early settling of cold disks. In the future, with large spectroscopic surveys such as 4MIDABLE-LR and the future Gaia Releases, it will be possible put even stronger constraints on first steps of the Milky Way formation, strongly complementing efforts being currently made at high-redshift.

Acknowledgements. We thank the E-science & IT team for COLAB service, computational clusters and research infrastructure at AIP. S.N. thanks Marica Valentini for the discussions on stellar ages. G.G. acknowledges support by Deutsche Forschungs-gemeinschaft (DFG, German Research Foundation) – project-IDs: eBer-22-59652 (GU 2240/1-1 "Galactic Archaeology with Convolutional Neural-Networks: Realising the potential of Gaia and 4MOST"). A.M. acknowledges support from the ERC Consolidator Grant funding scheme (project ASTEROCHRONOMETRY, G.A. n. 772293). This project has received funding from the European Research Council (ERC) under the European Union's Horizon 2020 research and innovation programme (Grant agreement No. 949173). This work has made use of data from the European Space Agency (ESA) mission *Gaia* (<https://www.cosmos.esa.int/gaia>), processed by the *Gaia* Data Processing and Analysis Consortium (DPAC, <https://www.cosmos.esa.int/web/gaia/dpac/consortium>). Funding for the DPAC has been provided by national institutions, in particular the institutions participating in the *Gaia* Multilateral Agreement.

References

- Abadi, M. G., Navarro, J. F., Steinmetz, M., & Eke, V. R. 2003, *ApJ*, 597, 21
- Anders, F., Chiappini, C., Santiago, B. X., et al. 2018, *A&A*, 619, A125
- Ardern-Arentsen, A., Monari, G., Queiroz, A. B. A., et al. 2023, *arXiv e-prints*, [arXiv:2312.03847](#)
- Astropy Collaboration, Price-Whelan, A. M., Lim, P. L., et al. 2022, *ApJ*, 935, 167
- Beers, T. C., Drilling, J. S., Rossi, S., et al. 2002, *AJ*, 124, 931
- Bellazzini, M., Massari, D., Ceccarelli, E., et al. 2023, *arXiv e-prints*, [arXiv:2312.02356](#)
- Belokurov, V. & Kravtsov, A. 2022, *MNRAS*, 514, 689
- Belokurov, V., Sanders, J. L., Fattahi, A., et al. 2020, *MNRAS*, 494, 3880
- Beraldo e Silva, L., Debattista, V. P., Nidever, D., Amarante, J. A. S., & Garver, B. 2021, *MNRAS*, 502, 260
- Bovy, J. 2015, *ApJS*, 216, 29
- Bressan, A., Marigo, P., Girardi, L., et al. 2012, *MNRAS*, 427, 127
- Buder, S., Sharma, S., Kos, J., et al. 2021, *MNRAS*, 506, 150
- Carollo, D., Christlieb, N., Tissera, P. B., & Sillero, E. 2023, *ApJ*, 946, 99
- Carter, C., Conroy, C., Zaritsky, D., et al. 2021, *ApJ*, 908, 208
- Chiba, M. & Beers, T. C. 2000, *AJ*, 119, 2843
- Conroy, C., Weinberg, D. H., Naidu, R. P., et al. 2022, *arXiv e-prints*, [arXiv:2204.02989](#)
- Creevey, O. L., Sordo, R., Pailler, F., et al. 2023, *A&A*, 674, A26
- da Silva, R., Porto de Mello, G. F., Milone, A. C., et al. 2012, *A&A*, 542, A84
- Dodd, E., Callingham, T. M., Helmi, A., et al. 2023, *A&A*, 670, L2
- Fernández-Alvar, E., Kordopatis, G., Hill, V., et al. 2021, *MNRAS*, 508, 1509
- Ferreira, L., Adams, N., Conselice, C. J., et al. 2022, *ApJ*, 938, L2
- Forbes, D. A. 2020, *MNRAS*, 493, 847
- Gaia Collaboration, Vallenari, A., Brown, A. G. A., et al. 2023, *A&A*, 674, A1
- Gallart, C., Bernard, E. J., Brook, C. B., et al. 2019, *Nature Astronomy*, 3, 932
- Gent, M. R., Eitner, P., Serenelli, A., et al. 2022, *arXiv e-prints*, [arXiv:2206.10949](#)
- Grisoni, V., Chiappini, C., Miglio, A., et al. 2023, *arXiv e-prints*, [arXiv:2312.07091](#)
- Guiglion, G., Nepal, S., Chiappini, C., et al. 2024, *A&A*, 682, A9
- Hopkins, P. F., Gurvich, A. B., Shen, X., et al. 2023, *MNRAS*, 525, 2241
- Horta, D., Schiavon, R. P., Mackereth, J. T., et al. 2023, *MNRAS*, 520, 5671
- Kartaltepe, J. S., Rose, C., Vanderhoof, B. N., et al. 2023, *ApJ*, 946, L15
- Kohandel, M., Pallottini, A., Ferrara, A., et al. 2023, *arXiv e-prints*, [arXiv:2311.05832](#)
- Lelli, F., Zhang, Z.-Y., Bisbas, T. G., et al. 2023, *A&A*, 672, A106
- Li, C., Yuan, Z., Monari, G., et al. 2023, *arXiv e-prints*, [arXiv:2311.15270](#)
- Limberg, G., Souza, S. O., Pérez-Villegas, A., et al. 2022, *ApJ*, 935, 109
- Lindgren, L., Bastian, U., Biermann, M., et al. 2021, *A&A*, 649, A4
- Mardini, M. K., Frebel, A., Chiti, A., et al. 2022, *ApJ*, 936, 78
- Matsunaga, N., Itane, A., Hattori, K., et al. 2022, *ApJ*, 925, 10
- McCluskey, F., Wetzel, A., Loebman, S. R., et al. 2023, *MNRAS*
- McMillan, P. J. 2017, *MNRAS*, 465, 76
- Miglio, A., Chiappini, C., Mackereth, J. T., et al. 2021, *A&A*, 645, A85
- Miglio, A., Chiappini, C., Mosser, B., et al. 2017, *Astronomische Nachrichten*, 338, 644
- Montalbán, J., Mackereth, J. T., Miglio, A., et al. 2021, *Nature Astronomy*, 5, 640
- Morrison, H. L. 1990, *JRASC*, 84, 107
- Naidu, R. P., Conroy, C., Bonaca, A., et al. 2021, *ApJ*, 923, 92
- Nepal, S., Chiappini, C., Guiglion, G., et al. 2024, *A&A*, 681, L8
- Nissen, P. E., Christensen-Dalsgaard, J., Mosumgaard, J. R., et al. 2020, *A&A*, 640, A81
- Norris, J., Bessell, M. S., & Pickles, A. J. 1985, *ApJS*, 58, 463
- Planck Collaboration, Ade, P. A. R., Aghanim, N., et al. 2016, *A&A*, 594, A13
- Queiroz, A. B. A., Anders, F., Chiappini, C., et al. 2023, *A&A*, 673, A155
- Queiroz, A. B. A., Anders, F., Santiago, B. X., et al. 2018, *MNRAS*, 476, 2556
- Recio-Blanco, A., de Laverny, P., Palicio, P. A., et al. 2023, *A&A*, 674, A29
- Rizzo, F., Vegetti, S., Fraternali, F., Stacey, H. R., & Powell, D. 2021, *MNRAS*, 507, 3952
- Rizzo, F., Vegetti, S., Powell, D., et al. 2020, *Nature*, 584, 201
- Robertson, B. E., Tacchella, S., Johnson, B. D., et al. 2023, *ApJ*, 942, L42
- Roman-Oliveira, F., Fraternali, F., & Rizzo, F. 2023, *MNRAS*, 521, 1045
- Schönrich, R., Binney, J., & Dehnen, W. 2010, *MNRAS*, 403, 1829
- Sestito, F., Longeard, N., Martin, N. F., et al. 2019, *MNRAS*, 484, 2166
- Sestito, F., Martin, N. F., Starkenburg, E., et al. 2020, *MNRAS*, 497, L7
- Sharma, S., Stello, D., Buder, S., et al. 2018, *MNRAS*, 473, 2004
- Skrutskie, M. F., Cutri, R. M., Stiening, R., et al. 2006, *AJ*, 131, 1163
- Soderblom, D. R. 2010, *ARA&A*, 48, 581
- Souto, D., Allende Prieto, C., Cunha, K., et al. 2019, *ApJ*, 874, 97
- Vitali, S., Slumstrup, D., Jofré, P., et al. 2024, *arXiv e-prints*, [arXiv:2401.02328](#)
- Xiang, M. & Rix, H.-W. 2022, *Nature*, 603, 599
- Zhang, H., Ardern-Arentsen, A., & Belokurov, V. 2023, *arXiv e-prints*, [arXiv:2311.09294](#)

Appendix A: Details on input parameters for StarHorse and kinematic calculations

The **StarHorse** Bayesian isochrone-fitting method (Queiroz et al. 2018, 2023) was used for the computation of the distances, extinctions and stellar ages with as noted in Sect. 2. We used the spectroscopic parameters from G23, galactic longitude (l) and latitude (b), photometric magnitudes G , B_p & R_p and parallaxes from *Gaia* DR3 along with parallax corrections by Lindegren et al. (2021) as inputs to **StarHorse**. We also used the infra-red photometry (JHKs) from Two Micron All Sky Survey (2MASS; Skrutskie et al. 2006). **StarHorse** then employs the Bayesian technique to match the observed data to the stellar evolutionary models from the PAdova and TRieste Stellar Evolution Code (PARSEC; Bressan et al. 2012). The isochrone ranges from 0.025 to 13.73 Gyr in age and -2.2 to $+0.6$ in metallicity. We do not adopt any prior for age as a function of $[Fe/H]$ or $[\alpha/Fe]$ (i.e., we do not force a high- $[\alpha/Fe]$ or metal-poor star to be old).

We used the 6D phase-space coordinates (sky positions, parallaxes, proper motions and radial velocities) from *Gaia* DR3 (Gaia Collaboration et al. 2023) along with the **StarHorse** distances to calculate positions and velocities in the galactocentric rest-frame. The integration of orbits was done with **Galpy** (Bovy 2015), a python package for Galactic dynamics calculations. We used **Astropy** (Astropy Collaboration et al. 2022) for coordinate and velocity transformations, assuming the Sun is located at radius $R_0 = 8.2$ kpc and the circular velocity of Local Standard of Rest (LSR) as $V_0 = 233.1$ km s $^{-1}$ (Bovy 2015; McMillan 2017). The peculiar velocity of the Sun with respect to the LSR is $(U, V, W)_\odot = (11.1, 12.24, 7.25)$ km s $^{-1}$ (Schönrich et al. 2010). To run **Galpy** we adopt the MW potential of McMillan (2017) and perform orbit integrations for a 3 Gyr period and save each orbit's trajectory every 2 Myr.

The guiding radius was computed as $R_g = L_Z/V_0$ and is independent of the axisymmetric potential. Here, L_Z is the star's instantaneous angular momentum, defined as $L_Z = R \cdot V_\phi$, where R is its galactocentric distance, and V_ϕ is its azimuthal velocity in the Galactic plane.

Appendix B: Validation of the StarHorse ages

B.1. Extending $[Y/Mg]$ chemical clock to old ages

Different chemical abundance ratios, such as the α -elements and the slow neutron-capture process (s-process) elements, owing to their distinct formation channels, display strong correlation with the age and have been widely used as chemical clocks (see e.g. da Silva et al. 2012; Queiroz et al. 2023 and references therein). The $[Y/Mg]$ chemical clock has been extensively studied and shows a well understood linear relation with no apparent variation with metallicity (Nissen et al. 2020). Nissen et al. (2020) using high-resolution and high Signal-to-Noise HARPS spectra for a sample of nearby solar-type stars studied the age-abundance relations. As a validation of the **StarHorse** ages for the MSTO-SGB stars we perform a test with this chemical clock.

We crossmatched our age sample stars with the GALAH DR3 catalog (Buder et al. 2021), to obtain the $[Y/Fe]$ and $[Mg/Fe]$ chemical abundances. We applied the recommended flags and quality cuts (see Buder et al. 2021) to obtain the good quality sample. We select stars with

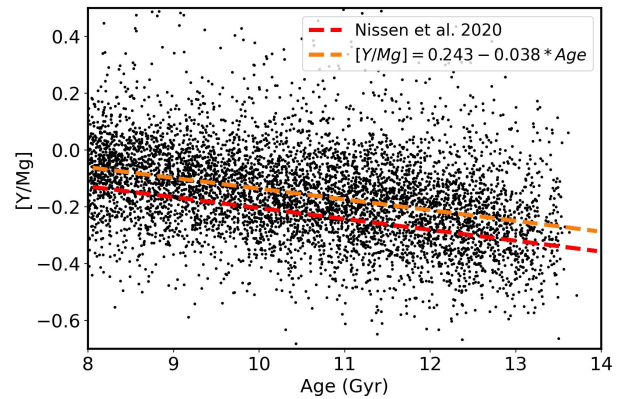


Fig. B.1: $[Y/Mg]$ versus the stellar age as a test of the **StarHorse** ages. The stars (black dots) were selected after a crossmatch with the GALAH DR3 catalogue (see text for details). The red dashed line represents the best fit line from Nissen et al. (2020) for a sample of nearby solar-twins and the orange line is our best fit for this data set. In this plot we extend the $[Y/Mg]$ chemical clock to the oldest ages and show that the **StarHorse** ages for the RVS-CNN catalogue are reliable at old ages with a good age resolution.

$[\alpha/Fe] < 0.15$ for this comparison, as 95% of (Nissen et al. 2020) solar-twin stars have $[Mg/Fe]$ below 0.15. Here, we focus on validation of **StarHorse** at the oldest age regime (> 8 Gyr) as the results of current work mostly focus on early epoch of MW. We have a sample of 6942 stars. In Fig. B.1 we plot $[Y/Mg]$ as a function of **StarHorse** ages. The red dashed line shows the best fit relation from (Nissen et al. 2020) given by $[Y/Mg] = 0.179 - 0.038 \cdot \text{Age}$. We perform a linear regression to obtain a fit for our stars, shown by the orange line; we obtain a fit of $[Y/Mg] = 0.260 - 0.038 \cdot \text{Age}$.

The chemical clock relation estimated from our stars using **StarHorse** ages and the GALAH abundances show a very close match to Nissen et al. (2020) relation and produce the same slope. The small shift in intercept reflects the systematic offset owing to different instruments and analysis pipelines and does not affect the conclusion. It is important to note that the Nissen et al. (2020) sample consisted of stars younger than 11 Gyr, here we extend this $[Y/Mg]$ chemical clock relation to the oldest ages with our old thin disc stars.

B.2. Test with confirmed GSE globular clusters and member stars.

A leaky-box chemical enrichment model has been widely used to describe the age-metallicity relationship of Globular Clusters (GCs) that are expected to be members of an accreted satellite galaxy (see e.g. Forbes 2020; Limberg et al. 2022). The leaky-box model is of the form $[Fe/H] = -p \cdot \ln(\frac{t}{t_f})$ where p is the effective yield of the system and t_f is the look-back time when the system first formed from non-enriched gas - the relation provides $[Fe/H]$ estimate as a function of stellar ages (t). The effective yield (p) of the satellite system is expected to be larger for galaxies with higher stellar mass. Here, we aim to test the reliability of our **StarHorse** ages by comparing the AMR described for the confirmed member GCs of

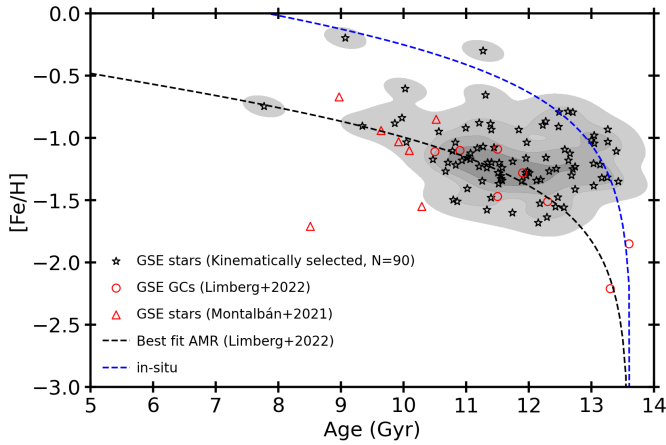


Fig. B.2: AMR for the GSE system. The red circles and the black curve show the GSE GCs from Limberg et al. (2022) and their best fit for the AMR. The blue curve represent the in-situ AMR. The red triangles represent the GSE stars from Montalbán et al. (2021). The black stars are the GSE candidates selected kinematically from our age sample (see text for details).

the Gaia-Sausage-Enceladus system identified by Limberg et al. (2022) and the GSE stars, with asteroseismic ages, identified by Montalbán et al. (2021). Limberg et al. (2022) calculated their ages for the GCs via CMD fitting.

In Fig. B.2 we present the AMR for the possible GSE members from our age sample. We select the GSE member stars by adopting $30 < \sqrt{J_r} < 50$ & $|L_z| < 500$ (see Limberg et al. 2022). We opt for only kinematic selection in favour of a statistically significant sample with ages. In the figure, the black dashed curve shows the AMR fit of (Limberg et al. 2022). A majority of our GSE candidates follow the AMR curve and show an excellent match similar to the GSE stars from Montalbán et al. (2021). We also plot the relation for in-situ GCs (blue curve) where some of our GSE candidates are located - this hints at possible contamination from in-situ stars. Some of these stars could initially be formed in the disc of MW and later splashed to hotter orbits (see Sec. 3.3). A further analysis of these stars require a clean selection with chemical abundances which are not currently available for these stars and is out of the scope of current work.

Our kinematically selected GSE candidates follow the AMR relation described for GSE Globular Clusters with ages and $[Fe/H]$ obtained via independent methods. This result shows that the StarHorse ages are reliable and have the necessary age resolution at this old age regime.

B.3. Test with isochrones

To validate the stellar ages provided by StarHorse we check for any effects of color-magnitude selection in the the Kiel diagram (T_{eff} vs $\log(g)$, Fig. B.3 top panel) and colour-magnitude diagram (CMD, Fig. B.3 bottom panel). We plot the stars belonging to the oldest age bin of 14–13 Gyr. The PARSEC stellar isochrones (Bressan et al. 2012), for ages 13 & 14 Gyrs and $[Fe/H]$ from -2.0 to 0.4 dex, which are also used by StarHorse, have been overplotted. The KDE distribution for the stars are well mapped by the stellar isochrones and show a very well-behaved distribution of the

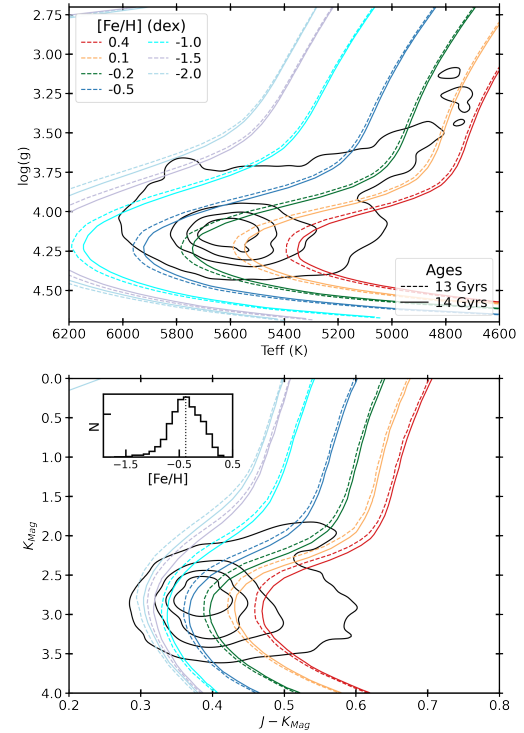


Fig. B.3: Kiel diagram and CMD for the 8078 stars of the age bin ($13 < \text{Age (Gyr)} < 14$). For illustration purpose, PARSEC stellar isochrones, for ages 13 & 14 Gyrs and $[Fe/H]$ from -2.0 to 0.4 dex are included. The CMD uses $JHKs$ absolute magnitudes from 2MASS which were used as inputs for StarHorse to estimate ages. The contour levels represent 25%, 50%, 75% and 100% of the distribution. In the bottom panel, the inset shows the MDF of the sample. The dotted line, at $[Fe/H] = -0.38$ represents the median $[Fe/H]$.

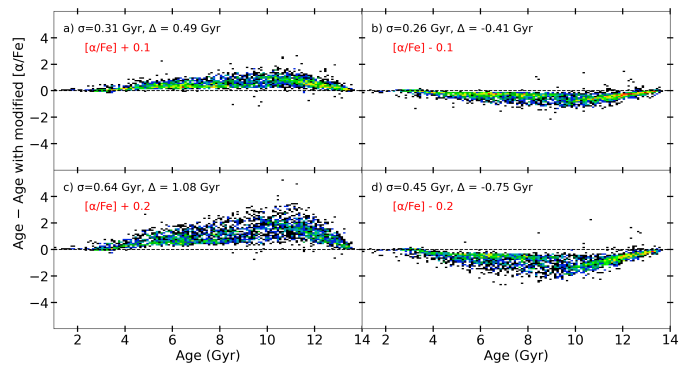


Fig. B.4: Influence $[\alpha/Fe]$ on StarHorse ages. We plot the age residuals, i.e. the difference of ages used in current study to the StarHorse ages with a modified alpha abundances, as function of the adopted ages. Each panel corresponds to the amount of change to the $[\alpha/Fe]$ (red, ± 0.1 and ± 0.2 dex). Mean scatter (σ) and the bias (Δ) are also calculated using a bootstrap sampling.

stars with no hard cuts that show possible systematic biases.

As reported in G23 and from our comparison with common GALAH DR3 Buder et al. (2021) stars we find the G23 $[\alpha/Fe]$ abundance for some MSTO stars could be underpre-

dicted by upto 0.08 dex compared to GALAH (the mean is estimated via the bootstrapping approach). The SGB stars do not show any bias. In case of open cluster, stars at the main-sequence turnoff are known to exhibit abundance differences (~ 0.05 to 0.30 dex) between the member stars as a function of their position on the Hertzsprung–Russell diagram (see Souto et al. (2019) and reference therein). Such an effect can also be expected for our MSTO stars.

Here, we perform a test to evaluate the influence of $[\alpha/\text{Fe}]$ abundance on the ages calculated by *StarHorse*. We take a set of 3000 stars from the age sample and alter their $[\alpha/\text{Fe}]$ values by ± 0.1 and ± 0.2 . In Fig. B.4 we show the results by plotting the age residuals as a function of the *StarHorse* ages used in this study. On increasing the $[\alpha/\text{Fe}]$ by $+0.1$ dex we find the residuals with a scatter of ~ 0.30 Gyr and observe a mean decrease in ages by ~ 0.50 Gyr while a change of -0.1 dex shows a mean increase in ages by ~ 0.40 Gyr. For a much larger increase in the $[\alpha/\text{Fe}]$ by $+0.2$ dex we find the residuals with a scatter of ~ 0.60 Gyr and observe a mean decrease in ages by ~ 1.0 Gyr while a change of -0.2 dex shows a mean increase in ages by ~ 0.75 Gyr. This test shows that the ages for the stars with a slight systematic bias in $[\alpha/\text{Fe}]$ could lead to a small over-prediction of the ages, however, this difference does not alter the results discussed in Sec. 3.

When using a maximum age limit of 13.73 Gyr (i.e. the age of the universe, Planck Collaboration et al. 2016), the posterior distribution function (pdf) by *StarHorse* for the oldest ages can be truncated. The latter will lead to underestimated uncertainties for the oldest ages. To estimate more realistic age uncertainties we perform a *StarHorse* run with a maximum age limit of 20 Gyr. In this case, we find a mean age uncertainties for stars older than 11 Gyr slightly higher at about 17%.

Appendix C: Properties of the metal-poor stars

C.1. Kinematics of the larger metal-poor sample

In this section we explore the kinematics of the larger metal-poor ($[\text{Fe}/\text{H}] < -1.0$) sample of stars that are confined to 3 kpc from the Galactic plane. Fig. C.1 shows the distribution of azimuthal velocity (V_ϕ) for the metal-poor (MP, panel a, $N=2950$) and very metal-poor (VMP, panel b, $N=748$) stars that are with $Z_{\text{max}} < 3$ kpc.

In panel a) we show the V_ϕ distribution of all MP stars (orange, dash-dot) and MP stars with cold orbits selected by eccentricity < 0.3 (blue, dashed). We consider $V_\phi < -50 \text{ km s}^{-1}$ as retrograde and $V_\phi > 50 \text{ km s}^{-1}$ as prograde orbits. For the low eccentricity subset (blue) we find a total 761 stars with 723 in prograde and 38 in retrograde orbits - this gives a prograde to retrograde (P/R) ratio of ~ 19 . This result supports the existence of our metal-poor thin disc discussed in Sec. 3.1 by showing an even larger number of MP stars in thin disc like orbits. For these low eccentricity stars, $\sim 25\%$ of the total, we find the V_ϕ peak at 190 km s^{-1} with the distribution skewed towards higher velocities. For all MP stars we find 2078 stars in prograde and 492 stars in retrograde giving $P/R \approx 4.2$. These MP stars are mostly old (see Sec. 3.2 and C.2). Hence, these results strongly support the presence of the Galactic disc at early epochs.

In panel b) we perform the similar examination as described above for the very metal poor stars ($[\text{Fe}/\text{H}] < -1.5$) in our sample. We have a total of 748 VMP stars with 121

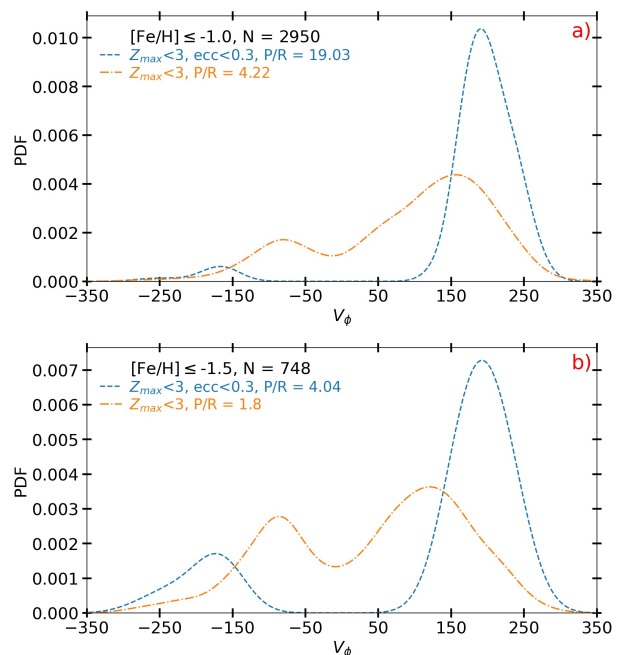


Fig. C.1: V_ϕ distribution for metal-poor stars confined to 3 kpc from the Galactic plane. a) V_ϕ distribution for the metal-poor ($[\text{Fe}/\text{H}] \leq -1.0$) set – full subset in yellow and the low eccentricity stars in blue. Ratio of prograde ($V_\phi > 50 \text{ km s}^{-1}$) to retrograde ($V_\phi < -50 \text{ km s}^{-1}$) stars is also shown. b) Same as above but for the very metal-poor ($[\text{Fe}/\text{H}] \leq -1.5$) subset. The prograde to retrograde ratio is provided for each sub sample.

stars in low eccentricity orbits. For all VMP stars we find 413 stars in prograde and 229 stars in retrograde giving a $P/R \approx 2$. For the low eccentricity stars we find 97 stars in prograde and 24 in retrograde giving a $P/R \approx 4$.

This analysis confirms the significant prevalence of prograde over retrograde disc-like stars for the MP and VMP stars and supports the discovery of our oldest thin disc in Sections 3.1 and 3.2.

C.2. Age of the metal-poor thin disc

In Fig. C.2 we present the distribution of ages for the metal-poor stars discussed in Section 3.1. This plot shows that the majority of the metal-poor stars in thin disc orbits (black) are exclusively older than 13 Gyr. There is a small number of stars younger than 13 Gyr, including a few younger than 9 Gyr – the latter we suspect being the population of young- $[\alpha/\text{Fe}]$ rich stars (see Grisoni et al. 2023 and references therein). The subset of slow rotating stars (orange) also shows a major peak older than 13 Gyr but has a significantly higher prevalence of stars younger than 13 Gyrs, indicating metal-poor stars younger than 13 Gyr mostly with slower azimuthal velocities. This hints at the a separate formation scenario for the older (> 13 Gyr) and the younger (< 13 Gyr) metal-poor stars. We note that when not using the age of the universe as a prior, we still find that metal-poor stars in thin disc orbits are dominated by systematically older stars in contrast to the stars with lower V_ϕ .

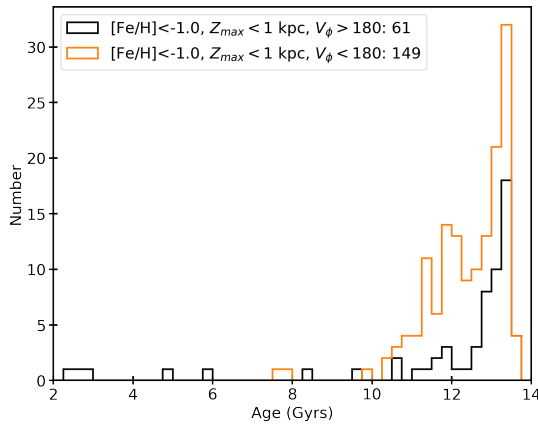


Fig. C.2: Distribution of the stellar ages for the metal-poor stars discussed in Sec. 3.1 - only stars present in the age sample are included. The metal-poor thin disc stars (black) and the other metal-poor stars with slower V_ϕ (orange) are shown along with the selection criteria and the number of stars with ages.

Appendix D: Orbital properties of the age sample

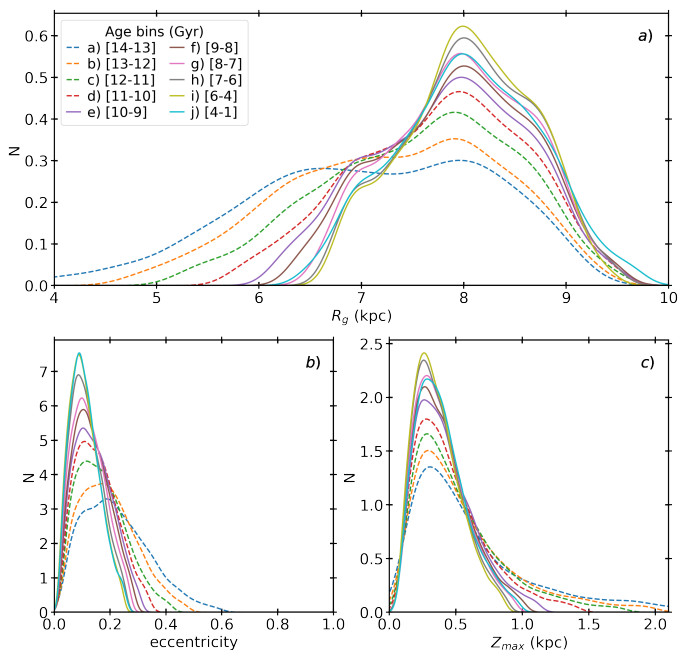


Fig. D.1: Orbital properties of the age sample stars in bins of stellar ages. a) The distribution of guiding radius (R_g) in age bins represented by the colors shown in the legend. b) Distribution of the orbital eccentricities. c) Distribution of the maximum excursion from the galactic plane (i.e. Z_{max}). Dashed lines represent the four oldest age bins.

In support to the idea that the old stars originated in the inner disc of the galaxy and are not the result of contamination from local stars with erroneous age estimation (see also Section 3.2) we present the orbital properties of the age sample.

In Figure D.1 we present the distribution of the orbital properties, represented by guiding radii (R_g), eccentricity and Z_{max} , of the age sample in different age bins. The

dashed lines represent the four oldest age bins and the solid lines represent the younger age bins (< 10 Gyr). Panel a) shows that for the oldest ages a large fraction of stars with inner guiding radius are seen. For younger ages (< 10 Gyr), we find most of the stars have $7 < R_g(\text{kpc}) < 9$. The eccentricity and Z_{max} distributions (in panel b and c), also show a major portion of stars at all ages in thin disc orbits, seen as low $\text{ecc} < 0.3$ and $Z_{max} < 0.5$ kpc. At the oldest bins (dashed lines) we see a significant fraction stars in warmer orbits owing to the high- $[\alpha/\text{Fe}]$ and the splash populations (see Section 3.3.1).

Appendix E: Old discs with external data sets

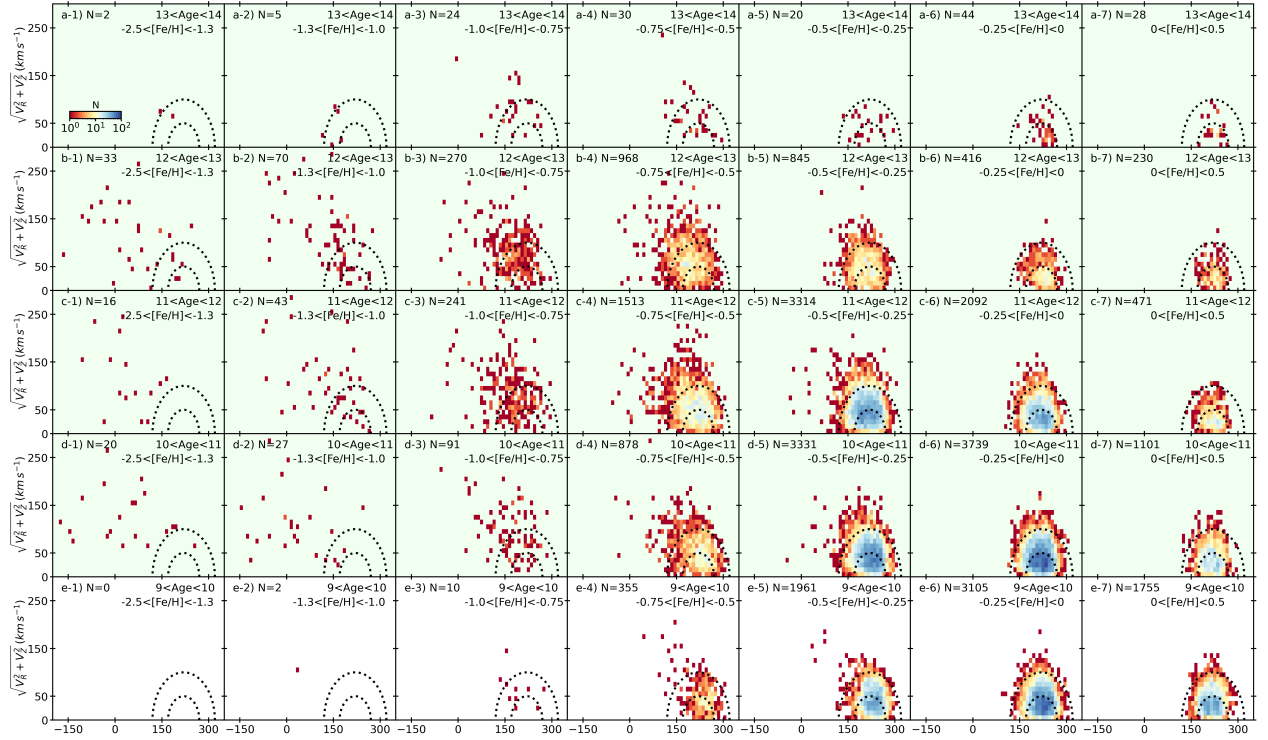
E.1. Using GALAH DR3 VACs

In this section we perform an external validation of our discovery of the old thin disc. We adopt the third data release catalogue of GALAH spectroscopic survey (Buder et al. 2021). In addition to the main catalogue with the spectroscopic parameters, Buder et al. (2021) also provide value added catalogues (VACs) with stellar ages, distances, kinematics and other derived parameters. The authors employ a similar bayesian method as adopted here. Their so-called Bayesian Stellar Parameters estimator (BSTEP, See Sharma et al. 2018 for details) adopts a different sets of priors compared to *StarHorse* - the most important difference, that is relevant to our current study, is an upper age limit of 13.18 Gyr instead of 13.73 Gyr. We note that imposing an age limit different than the ~ 13.8 Gyr age of the Universe (Planck Collaboration et al. 2016) can lead to systematic differences in the age span of the oldest components.

Our choice of GALAH DR3 for this validation is due to two factors. First, GALAH DR3 provides the largest sample of good quality MSTO+SGB stars compared to other high resolution surveys (see Table 1 of Queiroz et al. 2023). Second, this survey provides high quality radial velocity measurements - 99% of the MSTO+SGB sample have radial velocity uncertainties below 0.5 km s^{-1} . However, we note that after the application of the recommended flags and quality cuts (see Buder et al. 2021) and similar requirement on the uncertainties on the stellar parameters, ages and distances (see Sec. 2), we are left with 105 006 stars - this is half the size of our age sample.

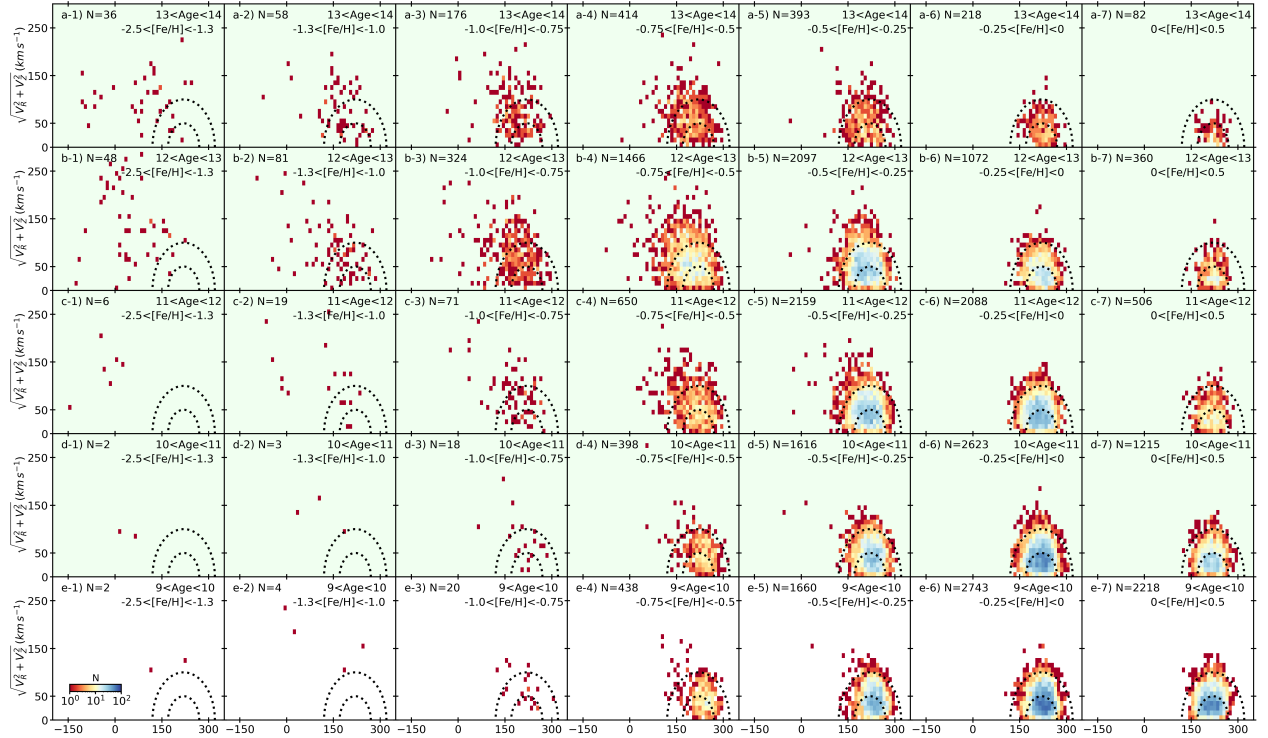
In Fig. E.1a we present the toomre diagram in bins of ages and metallicities similar to Fig. 2 using the $[\text{Fe}/\text{H}]$, ages and velocities from the GALAH DR3 catalogue. Similar to results discussed in Sec. 3.2, we find old stars in thin disc orbits covering the full range of metallicity (see panels a to d). Panels a-1 to a-7 show very few stars due to the upper limit of 13.18 Gyr employed by the BSTEP method. We re-calculated the ages for the the GALAH stars using *StarHorse*, with isochrones ranging to 13.73 Gyrs, and find the highest age bins better populated at all $[\text{Fe}/\text{H}]$ range as shown in Fig. E.1b.

Exploration of the old discs with GALAH DR3 VACs



(a) Toomre diagrams for the GALAH DR3 stars, using the [Buder et al. \(2021\)](#) catalogue, in bins of age and $[\text{Fe}/\text{H}]$ similar to Fig. 2.

Exploration of the old discs with GALAH DR3 StarHose ages



(b) Same as E.1a, for the same stars with [Buder et al. \(2021\)](#) $[\text{Fe}/\text{H}]$ and velocities, but with StarHose ages with isochrones ranging to 13.73 Gyr.

Fig. E.1: Toomre diagrams ($\sqrt{V_R^2 + V_z^2}$ vs. V_ϕ) for the GALAH DR3 stars in bins of $[\text{Fe}/\text{H}]$ and age.

E.2. Mass-[Fe/H] bias due to SGB/MSTO selection

In Fig. E.2 (panel a), we plot MDF for the four oldest bins of our age sample. We also show the MDF of the high- $[\alpha/\text{Fe}]$ (>0.15) stars, i.e., the chemical thick disk. Although the MDF for high- $[\alpha/\text{Fe}]$ stars significantly overlaps with that of the oldest bin (dashed blue), it is centered at $[\text{Fe}/\text{H}] \sim -0.5$ dex with a spread of ± 0.25 dex. The MDF for the oldest age bin, in addition to the spread at low $[\text{Fe}/\text{H}]$ similar to the high- $[\alpha/\text{Fe}]$ disc, shows a significant fraction of metal-rich stars. The mean $[\text{Fe}/\text{H}]$ gradually increases from -0.38 dex for 14–13 Gyr to -0.11 for 11–10 Gyr reflecting the rapid $[\text{Fe}/\text{H}]$ enrichment in the disc already in the first few Gyrs in the Galaxy. The similarity in the chemical space between the oldest thin disk and the chemical thick disk, makes it very difficult to disentangle these two stellar populations and highlights how crucial the stellar ages are in this case. This explains why previous analysis have missed the oldest disc.

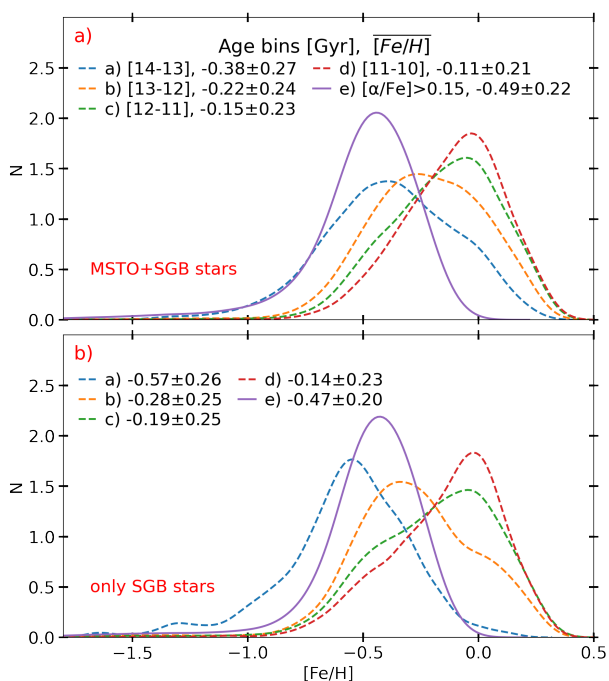


Fig. E.2: Metallicity distribution function (MDF) a): MDF for the old stars (>10 Gyrs, dashed) in bins of ages. The solid curve represents the high- $[\alpha/\text{Fe}]$ stars with $[\alpha/\text{Fe}] > 0.15$. The mean ($\overline{[\text{Fe}/\text{H}]}$) and spread of the MDF estimated via a bootstrap resampling with 5,000 iterations are listed. b): Similar to panel a, but only for the SGB stars in the age sample.

In Fig. E.2 (panel b) we now plot the MDF, similar to in panel a, for only the SGB stars. The MDFs now show a shift towards lower values and have the mean $[\text{Fe}/\text{H}]$ decreased. Using only SGB stars causes to bias against the old metal-rich stars. This finding can be understood in terms of stellar evolutionary timescales. As illustrated in Fig. B.3, the old metal-rich population is predominantly composed of main-sequence turn off stars. This is due to the fact that, at a given mass, the star's lifetime increases with metallicity. Even for the oldest age-bin, the subgiant phase is populated with masses exceeding 1.0 Msun, while lower masses remain in the Main Sequence (MS).

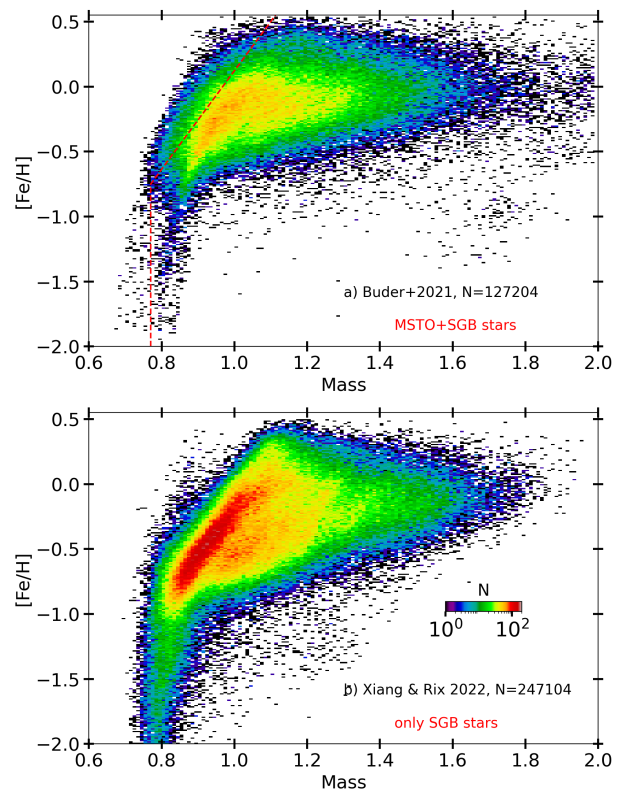


Fig. E.3: $[\text{Fe}/\text{H}]$ as a function of the stellar mass for the GALAH DR3 stars (panel a) and the LAMOST-LRS catalogue of Xiang & Rix (2022) (panel b). The plots are color-coded by logarithm of number density. The GALAH DR3 sample includes stars in both MSTO and subgiant evolutionary stages while the LAMOST sample only includes the subgiant stars. The red dashed lines plotted in panel a mark the visually estimated boundary from panel b. These plots show that the smaller sized GALAH DR3 sample includes significantly more low-mass stars at higher metallicities (>-0.5) compared to the larger LAMOST sample.

This effect is similarly observed in Fig. E.3, where we look at the mass- $[\text{Fe}/\text{H}]$ relations in external datasets. Here, we present two recent analysis with large spectroscopic surveys - the first with the GALAH DR3 VAC of Buder et al. (2021) in top panel and Xiang & Rix (2022) catalogue for the LAMOST low-resolution stars in bottom panel. The Xiang & Rix (2022) catalogue contains only the SGB stars while GALAH catalogue includes a mix of MSTO and SGBs. We see the lack of old metal-rich stars is evident in the Xiang & Rix (2022) catalogue in comparison to the GALAH sample.